Available online at www.sciencedirect.com
SCIENCE DIRECT®
Ultrasonics 41 (2003) 487–497
Ultrasonics
www.elsevier.com/locate/ultras

The wavelet response as a multiscale NDT method

Y. Le Gonidec, F. Conil, D. Gibert *

Géosciences Rennes (CNRS UMR 6118), Campus de Beaulieu, Université Rennes 1, 35042 Rennes Cedex, France

Received 14 March 2002; received in revised form 5 December 2002; accepted 29 January 2003

Abstract

We analyze interfaces by using reflected waves in the framework of the wavelet transform. First, we introduce the wavelet transform as an efficient method to detect and characterize a discontinuity in the acoustical impedance profile of a material. Synthetic examples are shown for both an isolated reflector and multiscale clusters of nearby defects. In the second part of the paper we present the wavelet response method as a natural extension of the wavelet transform when the velocity profile to be analyzed can only be remotely probed by propagating wavelets through the medium (instead of being directly convolved as in the wavelet transform). The wavelet response is constituted by the reflections of the incident wavelets on the discontinuities and we show that both transforms are equivalent when multiple scattering is neglected. We end this paper by experimentally applying the wavelet response in an acoustic tank to characterize planar reflectors with finite thicknesses.

PACS: 43.60; 43.40.L
Keywords: Acoustics; NDT; Multiscale; Wavelet transform

1. Introduction

Acoustical characterization is an important item in non-destructive testing of materials [23]. An often-used technique is the echographic one which consists of analyzing the waves reflected by the heterogeneities present in the material being tested. This approach is a very versatile one and its domain of applicability spans a huge scale range, from non-destructive imaging of integrated circuits, medical echography, to geophysical seismic imaging of the Earth's interior (e.g. [4,5,16]). The knowledge of the depth-dependent properties of the insonified material is another important issue. This may, for instance, concern the characterization of velocity gradients produced by diffusive chemical processes at interfaces, or the evaluation of the thickness of either heterogeneities or fractures embedded in the bulk material [22]. This goal generally involves sophisticated data analysis such as unstable processing issues like deconvolution needed to derive the reflectivity and nonlinear tomography and migration to derive the spatial variations of the mechanical parameters of the material.

In the present study, we propose a method called the "wavelet response" which enables an easy probing of the depth-dependent properties of material. This technique is very reminiscent of the wavelet transform [12] and allows for a direct assessment of the multiscale structure of the spatial variations of the acoustical properties. Also, this technique may be implemented in order to eliminate the need of delicate post-processing steps like deconvolution. The wavelet analysis is a multiresolution time-scale method which enables to perform a time-localized analysis of signals. Up to now, this method has been involved in the post-processing of acoustical signals in order to extract information like instantaneous frequency and evanescent properties [24], tiny echoes embedded in complex signals (e.g. [6]), or to suppress speckle noise (e.g. [1]). All these studies generally use classical analyzing wavelets like, for instance, the so-called Morlet's wavelet [9]. However, several authors recognized that particular classes of wavelets exist which may be given a deep physical sense. This has been found for the Poisson semi-group in potential field theory [8,21] and for the wave equation [17–19]. A deeper physical interpretation may be given to the wavelet transforms

* Corresponding author. Tel.: +33-2-2323-6091; fax: +33-2-2323-6090.
E-mail address: dominique.gibert@univ-rennesl.fr (D. Gibert).

0041-624X/03/$ - see front matter © 2003 Elsevier B.V. All rights reserved.
doi:10.1016/S0041-624X(03)00151-3

obtained with such physical wavelets (e.g. [25–27]). In the present paper, we show how the wavelet transform may be physically realized in an acoustical experiment in order to directly obtain the experimental wavelet transform of a physical system. In this first study, we choose to illustrate the principle of the method with a rather simple experiment where a reflected acoustical wave is used to assess for the thickness of a plate.

In the first part of this paper, we present the wavelet transform and show examples where it is used to perform a multiscale analysis of signals. The wavelet transform consists in correlating the analyzed signal with a family of wavelets obtained by dilating an oscillating function of finite duration. In this respect, the wavelet transform acts as a mathematical microscope [3] able to give a quantitative measure of the local appearance of a signal at different scales since wavelets are oscillating functions of constant shape whose width narrows as frequency increases (contrary to the windowed Fourier transform also known as the Gabor transform). In particular, we show how the geometrical characteristics may be inferred through the local regularity of the signal [2]. Synthetic examples of material structures are used to illustrate this approach.

In the second part of the paper, we introduce the wavelet response which consists in propagating a family of wavelets through the probed medium and constitutes a natural extension of the wavelet analysis (see for instance [14,25,26] in the case of homogeneous interfaces). When multiple scattering is neglected, both the wavelet transform and the wavelet response are shown to be equivalent, and the wavelet response may be interpreted with the conceptual framework of the wavelet transform.

The last part of the paper is devoted to an experimental realization of the wavelet response of plates immersed in a water tank. This simple experiment allows for a direct comparison with the synthetic examples discussed in the first two parts of the paper. Also discussed is the method used to implement the real-time wavelet response which prevents from further post-processing considerations.

2. Wavelet analysis of multiscale interfaces

2.1. Wavelet transform: principles

The wavelet transform was introduced in mathematical physics by Grossmann and Morlet [11], and the first studies concerned with the multiscale analysis of a complex signal s have been done by Mallat and Hwang [20]. In the present study, the analyzed signal is the acoustical impedance profile of the material. We shall define the continuous wavelet transform of s as a convolution product,

$$W[g,s](b,a) \equiv (D_a g * s)(b), \tag{1}$$

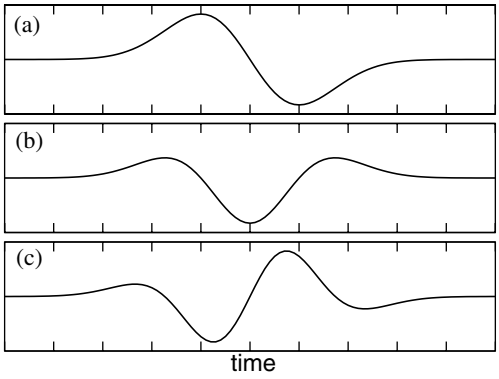

Fig. 1. Examples of analyzing wavelets: the first (a), second (b) (commonly referred to as the "*Mexican hat*" wavelet in the wavelet literature) and third (c) derivatives of a Gaussian function.

where b is a position variable for either space or time and g is the analyzing wavelet shown in Fig. 1. Any oscillating and localized function (i.e. with a compact or quasi-compact support) g with a vanishing integral may be an acceptable analyzing wavelet. A further property is the number of vanishing moments of g which controls the ability of the wavelet to detect more or less regular singularities present in the analyzed signal. The dilation parameter $a > 0$, and the dilation operator D_a acts as

$$D_a g(b) \equiv \frac{1}{a} g\left(\frac{b}{a}\right). \tag{2}$$

A particular class of functions of interest for the present study is the one whose members are the quasi homogeneous signals $s(b) = s_h(b) + p(b)$ where p is a polynomial of finite degree n, and s_h is an homogeneous function of homogeneity degree α, i.e. such that

$$s_h(\lambda b) = \lambda^\alpha s_h(b). \tag{3}$$

Provided the analyzing wavelet possesses a number of vanishing moments greater than n, the polynomial p will belong to the null-space of the wavelet transform, $W[g,p](b,a) = 0$. For such a quasi homogeneous function, Eq. (1) gives [12,13]:

$$W[g,s](\lambda b, \lambda a) = \lambda^\alpha W[g,s](b,a), \tag{4}$$

which means that the whole wavelet transform may be extrapolated over the entire half-space $(b, a > 0)$ from the wavelet transform given at a single dilation. The geometrical translation of this property is that the wavelet transform of a homogeneous function has a cone-like structure converging toward the homogeneity center of the analyzed function [20]. Moreover, the magnitude of the wavelet transform taken along any straight line crossing the homogeneity center follows a power law of exponent α with respect to dilation a [15]. When plotted in a log–log diagram, this power law becomes linear with a slope equal to the homogeneity degree α. The best signal-to-noise ratio is obtained for those straight lines corresponding to the maxima of the modulus of the wavelet

transform that are defined, following the definition used by Alexandrescu et al. [2], by the ridge function

$$r_j(a) \equiv |W[g,s](b_{\max,j},a)|, \quad (5)$$

that represents the absolute value of the wavelet transform taken along a given line of maxima where the variable $b_{\max,j}(a)$ is the position of the jth extrema of the dilated wavelet $D_a g$. The ridge functions automatically conform with the conical geometry of the wavelet transform. Moreover, to find the homogeneity centers, it is not necessary to localize them a priori so that it is very advantageous when studying wavelet transforms of complicated signals.

2.2. Singularities analysis by the wavelet transform

To illustrate the previous theoretical framework, we analyze three pure homogeneous singularities aimed at representing ideal reflectors. The first one is the Heaviside or step distribution which represents an ideal sharp transition between two homogeneous layers (bottom part of Fig. 2a). This homogeneous distribution corresponds to $\alpha = 0$ in Eq. (3). The modulus of its wavelet transform obtained with the analyzing wavelet shown in Fig. 1c is represented on the top part of Fig. 2a. We observe a cone-like geometry with lines of maxima converging toward the homogeneity center of the distribution, i.e. where the step occurs (the lines are not straight because of the log scale for the dilation axis). When plotted in a log–log diagram (Fig. 2b), the wavelet transform modulus taken along the lines of maxima (i.e. the ridge functions $r_j(a)$) follows a linear law and the ridge functions are horizontal straight lines in accordance with the theoretical homogeneity degree $\alpha = 0$.

The second example is the Dirac δ distribution of homogeneity $\alpha = -1$ which may represent an infinitely thin layer embedded in a homogeneous material. Again, the wavelet transform of this distribution possesses the typical conical geometry (Fig. 2c), and the ridge functions also appear as straight lines in a log–log diagram with the right slope $\alpha = -1$ (Fig. 2d).

The last example is the ramp function obtained by integrating the Heaviside distribution and whose regularity $\alpha = 1$. This model may, for instance, correspond to an impedance gradient associated with either diffusive chemical processes or with a density gradient corresponding to progressive compaction induced by increasing pressure in sedimentary layers. Corresponding to the transition between the overlying homogeneous layer and the gradient layer, this interface presents also a wavelet transform with a conical geometry pointing toward the interface (Fig. 2e) and possesses ridge functions with $\alpha = 1$ as expected (Fig. 2f).

These three examples show how the wavelet transform may be used to automatically detect and characterize sharp homogeneous changes present in a signal. The homogeneity center of the abrupt change is localized at the apex of the conical structure in the wavelet transform. The regularity α of the abrupt change may simply be estimated from the slope of the ridge functions $r_j(a)$ plotted in a log–log diagram.

We now turn to the analysis of clusters of homogeneous singularities. The first one is the Dirichlet window function obtained by merging two consecutive Heaviside distributions with opposite sign. The wavelet transform is shown on Fig. 3a and displays a more complicated pattern than the ones observed for the isolated singularities analyzed before. Indeed, depending on the dilation a, i.e. the scale at which the signal is analyzed, the wavelet transform either displays a single conical feature at large dilations where the window is seen as a whole, or displays two nearby cones at small dilations where the Heaviside steps are individually analyzed. A narrow intermediate dilation range $2^4 < a < 2^5$ centered on a critical dilation a_c separates the small- and large-dilation domains. The ridge functions plotted in a log–log diagram no more appear as straight lines and, instead, have a wiggly appearance (Fig. 3b). However, their asymptotic behavior at large and small dilations agrees with the results obtained for isolated pure singularities. For $a < 2^4$ two cones converge toward the edges of the window and the horizontal appearance of the ridge functions are typical of Heaviside-like events with $\alpha = 0$. For $a > 2^5$, the ridge functions also become linear with a negative slope $\alpha = -0.7$ indicating that the window begins to approximate a Dirac distribution. The intermediate dilation range $2^4 < a < 2^5$ corresponds to the anastomosis of the cones into a single one, and the ridge functions are no more linear. The critical dilation a_c provides an estimate of the size of the cluster, i.e. the width of the window function in the present example. Observe that the number n of ridge functions varies accordingly with the regularity of the abrupt changes detected. Indeed, $n = 3$ at small dilations (compare with Fig. 2a), and $n = 4$ at large dilation (compare with Fig. 2c). Note that the particular value of n depends on the number of extrema of the analyzing wavelet.

The second example is constructed with three nearby Heaviside distributions with the same sign, and has two characteristic scales (Fig. 3c). The smaller characteristic scale corresponds to the distance between adjacent steps and the larger is defined by the distance separating the two extreme steps. At small dilations $a < 2^3$, the wavelet transform displays three cones converging toward the individual Heaviside distributions, and the ridge functions are horizontal (Fig. 3d). At the large dilations $a > 2^6$, the wavelet transform reduces to a unique global cone and the ridge functions become progressively linear and horizontal with $\alpha = 0.1$ (Fig. 3d). This indicates that the global, large-scale, appearance of the signal is step-like. Outside of these extreme dilation domains, the ridge

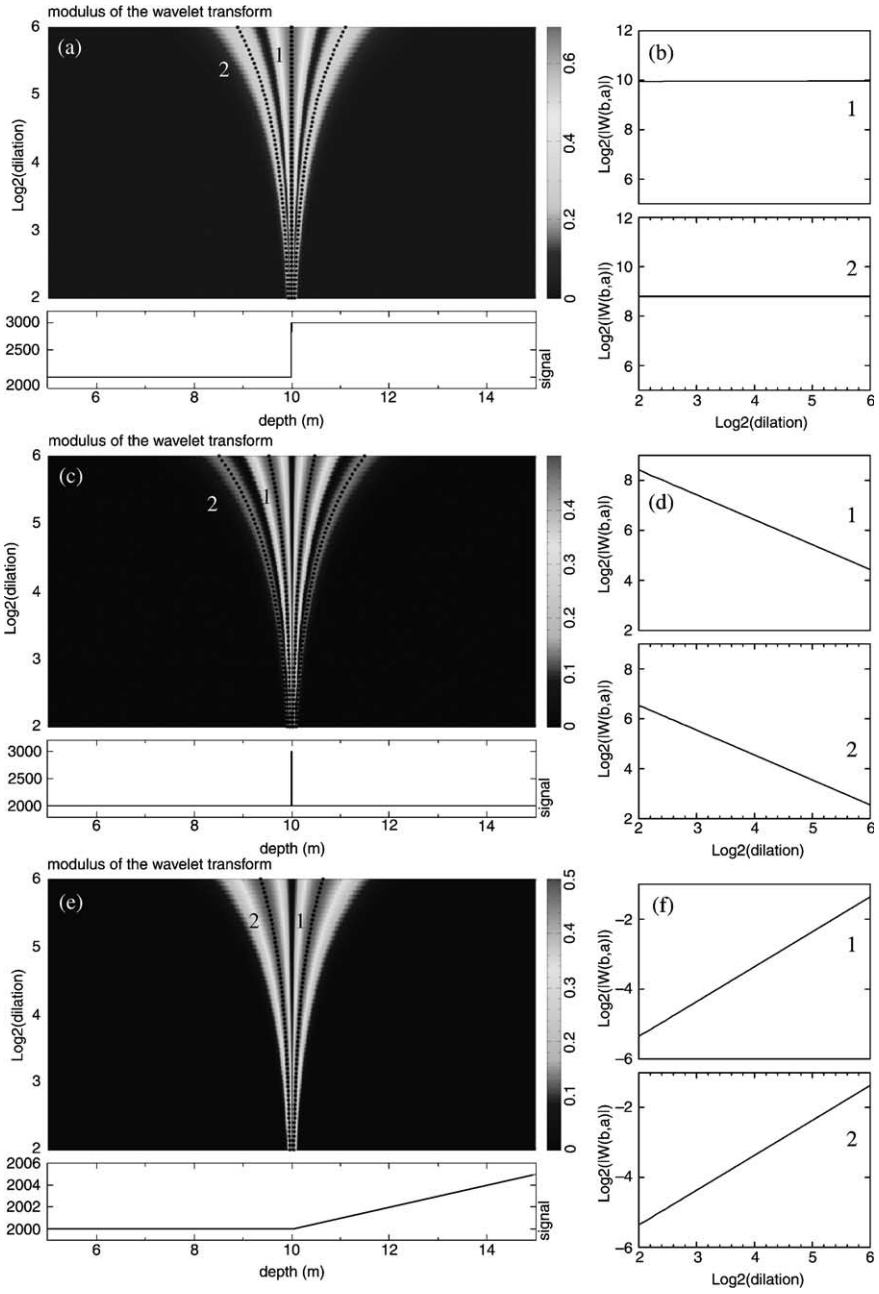

Fig. 2. The wavelet transform is obtained by convoluting the wavelet family with the space velocity profile. Left: Modulus of the continuous wavelet transforms of a Heaviside distribution (a), a Dirac distribution (c), and of a ramp function (e). The analyzing wavelet used is shown in Fig. 1c. The ridge functions (black dotted lines) converge toward the homogeneity center of the analyzed signal. The color scale is renormalized for each dilation in order to enhance the conical structure of the wavelet transform. Right: the $\log_2 - \log_2$ plots of labeled ridge functions of each wavelet transform are straight lines whose slope α equals the homogeneity degree of the detected singularity: (b) $\alpha = 0$, (d) $\alpha = -1$, (f) $\alpha = +1$.

functions cease to share a common appearance and their behavior depends on their position in the conical pattern seen in the wavelet transform. This makes the analysis more difficult. However, the external ridge functions located near the edges of the cone (like the leftmost one labeled 2 in Fig. 3d) clearly show the ramp-like appearance of the cluster for $2^4 < a < 2^5$ where $\alpha = 0.8$. Conversely, the internal ridges (like the central one labeled 1 in Fig. 3d) are more sensitive to the complicated anastomosis phenomena and no straight pattern may be seen in the intermediate dilation range $2^3 < a < 2^5$.

These examples show how the wavelet transform efficiently enhances the information about abrupt changes present in a signal by showing conspicuous cone-like patterns in the wavelet map. At observation scales where the abrupt changes appear homogeneous, the ridge functions follow a power law and varies linearly with respect to the dilation when plotted in a log–log diagram.

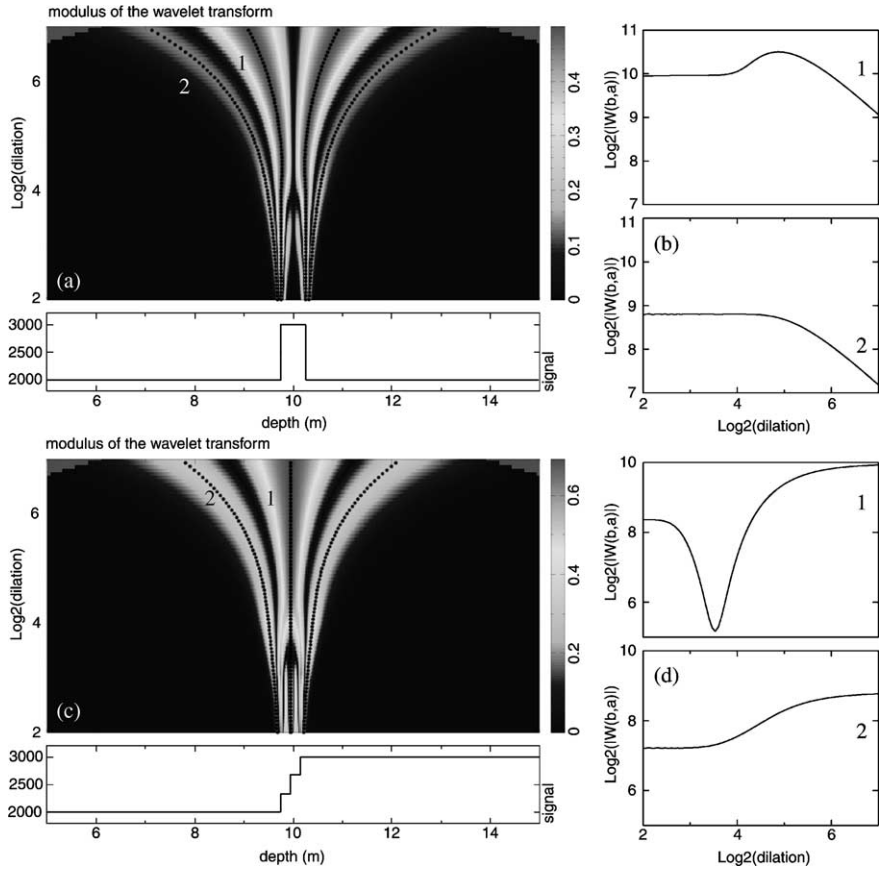

Fig. 3. (a) Normalized modulus of the wavelet transform of a window function. (b) $\log_2 - \log_2$ plot of the two leftmost ridge functions of the wavelet transform shown on (a). For $a < 2^4$, the ridge functions are horizontal with $\alpha = 0$, and for $a > 2^5$ the slope $\alpha = -0.7$ is more typical of a Dirac-like singularity. (c) Modulus of the wavelet transform of a signal composed of three successive Heaviside distributions. (d) $\log_2 - \log_2$ plot of the two leftmost ridge functions of the wavelet transform shown on the left. The ridge function labeled 1 shows the three scale-dependent appearances suggested by the structure of the wavelet transform. The small-dilation part of this ridge function indicates $\alpha = 0$, the intermediate one $\alpha = 0.8$, and the large one $\alpha = 0$.

For clusters of nearby singularities (Fig. 3), the wavelet transform possesses a hierarchical arrangement of conical patterns which constitute a means to probe the multiscale nature of the cluster. This hierarchical arrangement is also present in the ridge functions which appear wiggly with straight segments in limited dilation ranges where the analyzed signal locally appears homogeneous.

3. Wavelet response of multiscale interfaces

3.1. Wavelet response: definition

We now show how the principles of the wavelet analysis explained above may be extended to remotely probe an acoustical impedance profile by propagating a family of wavelets through the material. Mathematically, this consists of replacing the convolution operator of Eq. (1) by the propagator operator. This will led to what will be referred to as the "wavelet response" obtained by recording the reflected wavefields for a family of source wavelets. In accordance with the notations of Eq. (1), the 1-D wavelet response is defined as

$$R[g,s](b,a) \equiv (D_a g \otimes s)(b), \tag{6}$$

where the symbol $\otimes$ represents the 1-D propagation of the dilated wavelet $D_a g(t)$ through the velocity profile $s(z)$. Physically, the wavelet response represents the reflected time-varying wavefield recorded at a given depth z_r, the source wavelet being emitted at depth z_s. Both the source and the recording points are assumed to be located on the same side of the reflector to be probed.

The position variable b does not have the same physical meaning for the wavelet transform where it represents depth and for the wavelet response where it represents the two-way flight time of the recorded waves composing the wavelet response. So, both transforms are not in the same physical spaces and not directly comparable. However, a link between the wavelet response (6) and the wavelet transform (1) may be established when multiple scattering is neglected. Let us introduce the reflectivity function $r(t)$ defined as being the reflected wavefield corresponding to a Dirac source

(e.g. [10]). The reflectivity is then a Green's function, and we have,

$$R[g,s](t,a) = (D_a g * r)(t), \tag{7}$$

where the reflectivity

$$r(t) \equiv \frac{1}{2}\frac{\mathrm{d}}{\mathrm{d}t}\ln\gamma(t), \tag{8}$$

with the acoustical impedance $\gamma(t) = \rho(t)s(t)$. The correspondence from depth to time is given by

$$t(z) = \int_{z_s}^{z} s^{-1}(\xi)\,\mathrm{d}\xi + \int_{z_r}^{z} s^{-1}(\xi)\,\mathrm{d}\xi. \tag{9}$$

Assuming a constant density ρ, and using Eq. (9) to flip from temporal to spatial derivative, we get from Eq. (8):

$$r(t) = \frac{1}{4}\frac{\mathrm{d}}{\mathrm{d}s}s[z(t)], \tag{10}$$

and Eq. (7) becomes,

$$R[g,s](b,a) \equiv \left(D_a g * \frac{\mathrm{d}}{\mathrm{d}z}s[z(t)]\right)(b). \tag{11}$$

A comparison of Eqs. (1) and (11) shows that, when both multiple scattering and density variations are neglected, the wavelet response of the velocity profile s is the wavelet transform of the first space-derivative of the velocity profile. If multiple scattering cannot be neglected, the reflected wavefield is much more complicated than the reflectivity and huge discrepancies appear between the wavelet transform and the wavelet response.

The analyzing wavelet shown in Fig. 1b is the integral of the wavelet used for the wavelet analysis. This choice has the advantage to produce the same number of ridge functions in both the wavelet transform and the wavelet response and allows a direct comparison between both transforms. Moreover, in order to obtain the same slope α as for the wavelet transform, each line of the wavelet response has been multiplied by the dilation a in the following examples. In practice, each horizontal line of the wavelet response map is actually obtained by propagating (using a finite difference method) a wavelet of dilation a and recording the corresponding reflected response. The whole wavelet response is then a stack of such traces arranged with increasing dilation in order to obtain a picture similar to a wavelet transform. All wavelet responses shown in this paper are such that the source and the receiver points are located at the same place (i.e. $z_r = z_s$). Moreover, since the source wavelet is causal, each trace of the wavelet response is shifted by the half-duration of the source wavelet in order to produce pictures similar to those obtained for the wavelet transform.

3.2. Wavelet response of multiscale reflectors

The first application is done on the window function whose wavelet response (Fig. 4a) has a conical structure with four ridge functions at large dilations, typical of a Dirac distribution (compare with Fig. 2c). At small dilations, and as observed in the wavelet transform of the window (Fig. 4a), the main cone of the wavelet response splits into two cones pointing toward the edges of the window and counting three ridge functions typical of a Heaviside distribution (compare with Fig. 2a). This twofold appearance of the window also exists in the log–log plots of the ridge functions (Fig. 4b) which are flat with $\alpha \simeq 0$ at small dilations and monotonically decrease with $a \simeq -0.85$ at large dilations. In the intermediate dilation range, the ridge functions do not display a well-defined slope because of complicated interference phenomena between the two sub-cones. The wavelet response then allows the quantitative assessment of the multiscale nature of the reflector by indicating that for high-frequency (i.e. small dilations) wavelets, the reflector appears as two separated step-like reflectors while at low frequency (i.e. large dilations), the same structure appears as a Dirac-like reflector. As for the wavelet transform, the outer ridge functions located on the edges of the cone (i.e. lines 2 and 3) are less wiggly than the inner ridge functions (i.e. lines 1 and 4) which are more affected by interference phenomena. Let us remark that, contrarily to the wavelet transform which is symmetrical, the ridge functions of the wavelet response are non-symmetrical (i.e. lines 2 and 4 differ from lines 1 and 3 respectively) because the wavelet response is polarized (i.e. the reflected wave forming the wavelet response are coming from the right since the source and the receiver are located at the very left of the velocity profile). The corner dilations corresponding to the upper end of the small-dilation range are different for the outer ridges ($a_c = 2^{-11}$) and for the inner ridges ($a_c = 2^{-11.5}$). Since the inner ridges are mostly affected by the internal interference phenomena occurring in the fine structure of the reflector, their corner dilations are a good indicator of the size of the structure. Indeed, the corner wavelength (simply obtained by multiplying the dilation with velocity) corresponding to $a_c = 2^{-11}$ is $\lambda_c = 1$ m which is twice the width of the window reflector used in this example.

The second example concerns the cluster of Heaviside velocity jumps already shown in Fig. 4c and having two characteristic scales defined by the interval between adjacent steps and by the overall width of the reflector. The large-dilation part $a > 2^{-10.5}$ of the wavelet response is a single cone with three ridge functions typical of a Heaviside distribution. At intermediate dilations $a \simeq 2^{-11}$ this cone is split into two cones with two ridges each, and at smaller dilations $a < 2^{-11.5}$ these two cones disappear while more ridges appear. This threefold appearance of the wavelet response is present in the log–log plots of the inner ridge function (labeled 3 in Fig. 4d). The outer ridges of the main cone (ridges 1 and 2 in Fig. 4d) are less affected by the interference phenomena

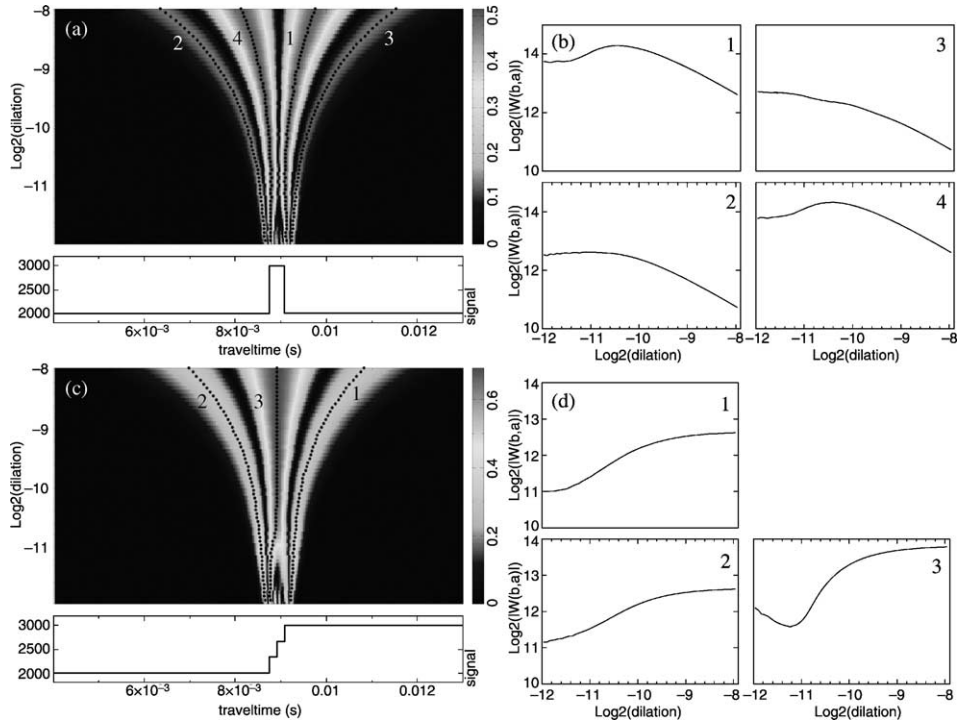

Fig. 4. The wavelet response is obtained by propagating the temporal wavelet family in the velocity profile. (a) Modulus of the wavelet response of a window function. The analyzing wavelet is the one shown in Fig. 1b. (b) $\log_2 - \log_2$ plot of the main four ridge functions of the wavelet response displayed in (a). (c) Modulus of the wavelet response of a signal composed of 3 nearby Heaviside steps. (d) $\log_2 - \log_2$ plot of the main 3 ridge functions of the wavelet response displayed in (c). The results are equivalent to the one presented in Fig. 3 when multiple scattering is neglected.

and display the simplest behavior with a flat appearance at small ($a < 2^{-11.5}$) and large ($a > 2^{-9.5}$) dilations and a positive slope at intermediate dilations. This is consistent with the wavelet analysis of the same signal (Fig. 3d) which indicates that this multiscale signal has a Heaviside-like appearance at small and large dilations and a ramp-like behavior at intermediate dilations. The inner ridge function provides a corner dilation $a_c = 2^{-11.5}$ which corresponds to a corner wavelength $\lambda_c = 1$ m indicating a width of the reflector equal to half a meter.

The wavelet response of the two multiscale synthetic signals considered in this section is consistent with the results obtained with the wavelet analysis of the same signals. In particular, we observe that the asymptotic appearance of the signals at very small and very large dilations is the same for both the wavelet transform and the wavelet response indicating that neglecting multiple scattering seems valid and that the convolution approximation (11) of the wavelet response is acceptable. The ridge functions extracted from the wavelet response look very similar to the one obtained with the wavelet transform with second-order discrepancies due to the non-symmetrical nature of the wavelet response and to interference phenomena occurring at medium dilations. The wavelet response then constitutes a tool to remotely probe both the coarse and the fine structure of a reflector. The slopes derived from the outer ridge functions are most useful to infer the fine-scale and global-scale features of the reflector, and the corner dilations identified in the log–log plots of the inner ridge functions provide information about the width of the reflector.

4. Application: wavelet response of planar interfaces

4.1. Experimental setup and wavelet response

In this section, we present an experimental realization of the wavelet response presented above. As stated in Section 1, this allows for a real-time implementation of the wavelet response which enables a rapid and eventually automatic detection and characterization of reflectors. The experiments shown here have been done in a water tank, and the reflector was simply constituted by plates of finite thicknesses (Fig. 5). This is aimed at experimentally reproducing the synthetic example presented above and concerning the window interface. These experiments could for instance correspond to the remote probing of an open fracture in an otherwise homogeneous medium.

The first part of the experiment is to build the wavelet family to be propagated through the probed medium. This is done by calibrating the whole apparatus chain so that, when propagated through water, the wavelet family remains unchanged. This reference wavelet

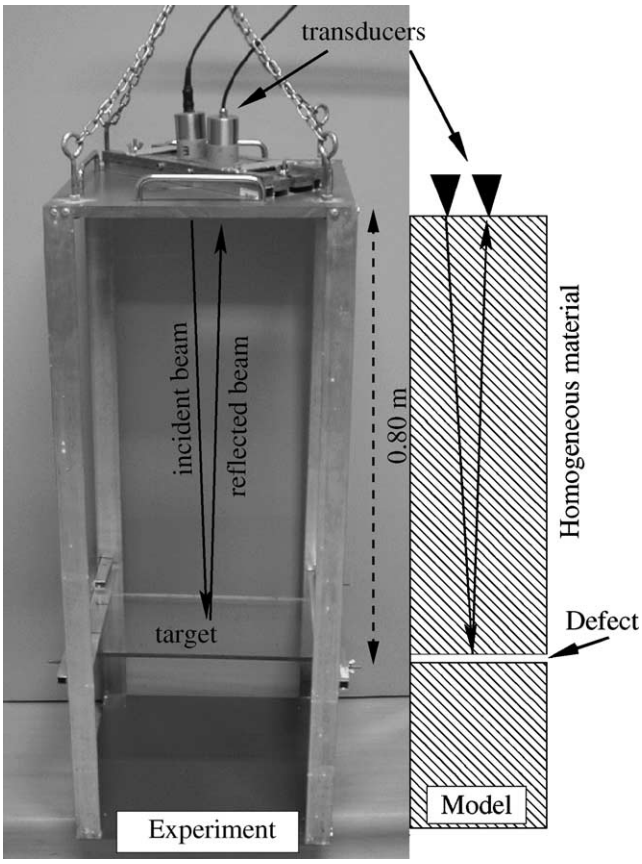

Fig. 5. Experimental setup used to perform multiscale ultrasonic probings. The whole apparatus is immersed in a water tank (5 m^3). The target (polycarbonate plates with thicknesses of 1, 2, 4 and 8 mm) models an open fracture in a homogeneous material. The piezoelectric transducer (four pairs to span the frequency range from 150 kHz to 1.2 MHz) are tilted in order to align their beams on a common incident spot.

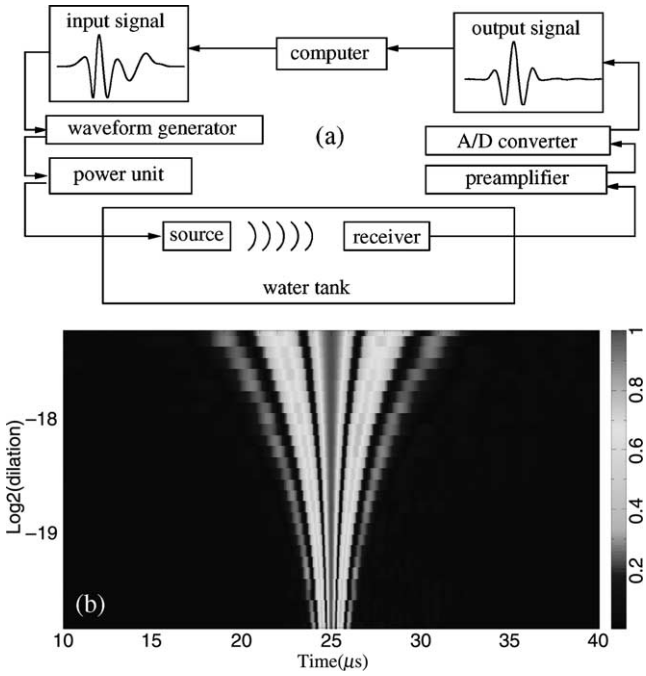

Fig. 6. (a) Schematic view of the setup used to construct the experimental wavelet response. A non-linear inverse method [7] is used to find the numerical input signal (top left) to send to the arbitrary waveform generator in order to obtain an output signal (top right) equals to a pure wavelet chosen to be a dilated version of the fourth derivative of a Gaussian $d^4/dt^4\, e^{-t^2}$. (b) In this way, the wavelet family (28 wavelets) is constructed and represented by the modulus of the wavelet response obtained by propagating the source signals through water. The dilation $a = f_c^{-1}$ where f_c is the main frequency of the wavelets which are dilated versions of the fourth derivative of a Gaussian.

response could in principle be obtained by deconvolving the reflected waves produced by a pulse source with a broad frequency. However, both non-linearities of the apparatus (especially at large source power) and numerical instabilities produced by noise during the deconvolution make this method too inaccurate. In practice, we observed that much more accurate results are obtained by using a family of source signals such that the received signals are the sought wavelets. This is practically implemented by searching for the numerical source signals to be sent to the arbitrary waveform generator in order that the output signals recorded with the receiving transducer are an imposed wavelet family (Fig. 6a). This is performed through a non-linear inverse method based on simulated annealing and neural network [7]. In the present instance, the analyzing wavelet is the fourth derivative of a Gaussian (Fig. 1). Following this procedure, a family of input signals was constructed for four pairs of transducers with central frequencies $f_c = 250$, 500, 750, and 1000 kHz. For convenience, the output wavelets are such that the dilation $a = f_c^{-1}$ where the central frequency with maximum energy f_c is given in Hz. Fig. 6b shows the so-obtained wavelet family. We emphasize that neither deconvolution nor further processing were applied to the received signals which, as shown in Fig. 6b, are as they are captured by the receiving A/D converter. Another advantage of this approach is that, once the source signals have been found, the wavelet responses are obtained in real time. This allows for both an immediate control of the quality of the data and assessment of the signal-to-noise ratio.

The experimental setup consists of a rigid frame holding a pair of ultrasonic transducers and the target to be analyzed (Fig. 5). The targets are polycarbonate plates with thicknesses of 1, 2, 4 and 8 mm. By combining the available frequencies (150 kHz–1.2 MHz) and plate thicknesses, and by appropriately rescaling the data, it is possible to merge the data into a single data set spanning 5 dilation octaves in the wavelet response. The wavelet family used in this experiment counts 28 wavelets, and the wavelet response of the plates was obtained by stacking the received signals in order to enhance the signal-to-noise ratio. This wavelet response is shown in Fig. 7a.

4.2. Results and discussion

The experimental wavelet response appears like the synthetic wavelet response of a window function (Fig. 4a) with a single conical pattern at large dilations and two small cones pointing toward the faces of the plate at small dilations. The experimental ridge functions (Fig. 7b) have a flat horizontal part at small dilations typical of a Heaviside distribution. At intermediate dilations the ridge functions are wiggly because of complicated interferences occurring inside the reflector (i.e. the plate). The critical dilation $a_c = 2^{-19}$ where this part of the ridge functions begins is an indicator of the thickness of the reflector. Indeed, a_c corresponds to a wavelength $\lambda_c = 4.2$ mm in the polycarbonate, a value about twice the thickness of the plate. At large dilations $a > 2^{-17.5}$ the ridge functions again become linear with a negative slope $\alpha \simeq -0.6$ indicating that, at large scales, the reflector has a Dirac-like appearance. A numerical wavelet response done with the same parameters as those of the water tank experiment produces ridge functions in very good accordance with the experimental ones (Fig. 7c).

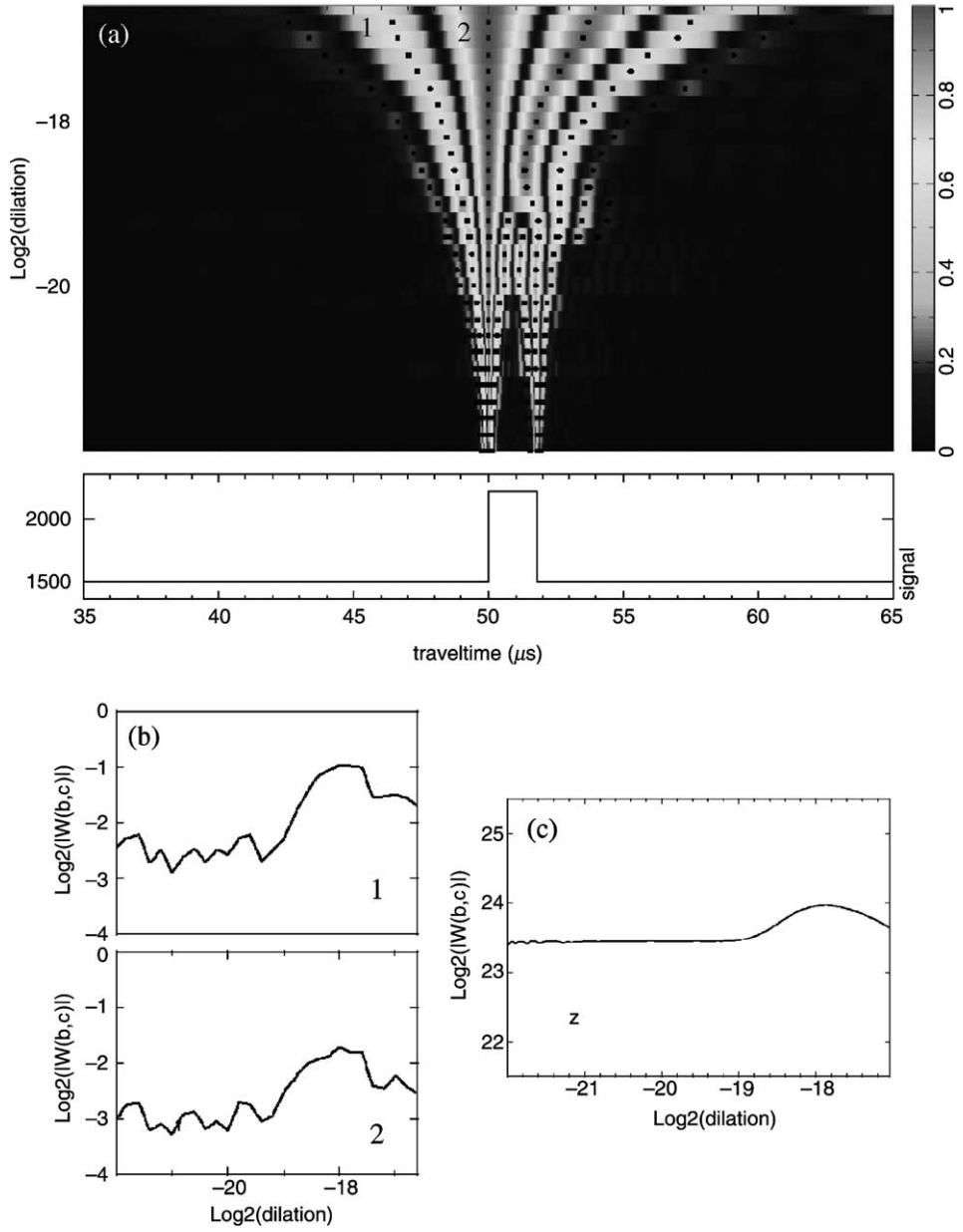

Fig. 7. (a) Modulus of the experimental wavelet response of a polycarbonate plate immersed in water. At large dilations, the wavelet response resembles that of a Dirac distribution while, at small dilations, two cones point towards the faces of the plate and count one less ridge function. (b) $\log_2 - \log_2$ plot of two ridge functions of the wavelet response displayed in (a). (c) Synthetic ridge function obtained by performing a 1-D numerical wavelet response with parameters identical to those of the water tank experiment.

5. Conclusion

We have shown how the wavelet transform can be used to identify and characterize reflectors present in a material. These reflectors produce conspicuous cone-like patterns in the wavelet transform with their apex pointing toward the homogeneity centers of the singularities. A local analysis of each abrupt change is possible by using the ridge functions extracted from the modulus of the wavelet transform. The global appearance of multiscale clusters of abrupt changes is characterized in the large-dilations domain $a > a_c$ by the slope α of the ridge functions which appear almost straight when plotted in a log–log diagram. At these global scales, an interface may be considered as a single abrupt change with regularity α. At finer dilations $a < a_c$ the ridge functions eventually cease to be straight and the reflector must instead be seen as a cluster of small-scale features with their own cone-like pattern in the wavelet transform. Despite complicated interference phenomena among the individual cones, which generally precludes the analysis of each small-scale event, the overall size of the cluster may be estimated from the corner dilation a_c at which the large-scale behavior of the interface ceases to hold.

The wavelet response is an experimental extension of the wavelet transform when the signal to be analyzed (i.e. the velocity profile of the medium) cannot be directly convolved with the wavelets but can only be remotely probed by propagating wavelets into the material. The reflected waves produced by the impinging of the incident wavelets onto the reflectors present in the medium constitute the wavelet response. We have shown that the two transforms are equivalent when multiple scattering is neglected. As for the wavelet transform, cone-like features and ridge functions can be recognized in the wavelet response, and applications of the wavelet response reveal that useful informations can be obtained about complex interfaces, namely: the large-scale regularity of the single equivalent interface and the size of the cluster of the small-scale variations forming the global interface. Surprisingly, the wavelet response can be analyzed over a narrower dilation range than the one necessary in the wavelet transform (4 octaves against 6). Thanks to numerically controlled piezoelectric transducers, a family of wavelet sources can be directly emitted by the experimental setup in order to probe a reflector in real time. The experimental results obtained for targets made of polycarbonate plates totally agree with the numerical examples and give an insight on how to design and built sounding devices able to characterize material defects.

The practical application of the method depends on the possibility to obtain the wavelet response of the reference medium where no target to detect exists. For absorbing reference media, the wavelet response may be obtained by adjusting the power of the source at the highest frequencies where absorption is maximum. For heterogeneous media, the wavelet response may only be obtained in a mean-field sense in order to remove the speckle pattern. This implies the medium of interest to be stationary over a sufficiently long distance. Several geophysical situations provide the necessary condition for the wavelet response analysis to be used. This is for instance the case of both marine seismics and sonar probing whose experimental contexts are very reminiscent of the experiment performed in the acoustical tank. Furthermore, wide-band acoustical sources are available to cover a significant frequency range. Another situation of interest is borehole imaging where wide-band sources may again be used and where relatively homogeneous reference media are found. These experimental situations are currently addressed and will be presented in forthcoming studies.

Acknowledgements

We thank Michel Lemoine for his skilled assistance in designing the experimental setup. Associate Editor Peter Nagy made very constructive comments. This work is financially supported by the CNRS and ANDRA through the GdR FORPRO (Research action number 99.II) and corresponds to the GdR FORPRO contribution number 2002/04 A.

References

[1] A. Abbate, J. Koay, J. Frankel, S.C. Schroeder, P. Das, Signal detection and noise suppression using a wavelet transform signal processor: Application to ultrasonic flaw detection, IEEE Trans. Ultrason. Ferroelectrics Frequency Control 44 (1997) 14–26.
[2] M. Alexandrescu, D. Gibert, G. Hulot, J.-L. Le Mouël, G. Saracco, Detection of geomagnetic jerks using wavelet analysis, J. Geophys. Res. 100 (1995) 12557–12572.
[3] F. Argoul, A. Arnéodo, G. Grasseau, Y. Gagne, E.J. Hopfinger, U. Frisch, Wavelet analysis of turbulence reveals the multifractal nature of the Richardson cascade, Nature 338 (1989) 51–53.
[4] U. Bernini, P. Momile, A. Novellino, P. Russo, Photoacoustic imaging of layered microcircuits for non-destructive evaluation of sub-surface defects, J. Mater. Process. Technol. 54 (1995) 181–185.
[5] M.G. Bostock, Seismic imaging of lithospheric discontinuities and continental evolution, Lithos 48 (1999) 1–16.
[6] M. Castillo, E. Moreno, J. Solano, O. Sánchez, M. González, M. Rodríguez, Ultrasonic flaw detection in cast iron using a multiresolution analysis, Instrum. Develop. 3 (1998) 27–31.
[7] F. Conil, D. Gibert, F. Nicollin, Non-linear synthesis of input signals in ultrasonic experimental setups, J. Acoust. Soc. Am., in press.
[8] D. Gibert, M. Pessel, Identification of sources of potential fields with the continuous wavelet transform: application to self-potential profiles, Geophys. Res. Lett. 28 (2001) 1863–1866.
[9] P. Goupillaud, A. Grossmann, J. Morlet, Cycle–octave and related transforms in seismic signal analysis, Geoexploration 23 (1984) 85–102.

[10] S.H. Gray, N. Bleistein, Imaging and inversion of zero-offset seismic data, Proc. IEEE 74 (1986) 440–456.
[11] A. Grossmann, J. Morlet, Decomposition of Hardy functions into square integrable wavelets of constant shape, SIAM J. Math. Anal. 15 (1984) 723–736.
[12] A. Grossmann, Wavelet transform and edge detection, in: M. Hazewinkel (Ed.), Stochastic Processes in Physics and Engineering, D. Reidel, Norwell, Mass, 1986, pp. 149–157.
[13] A. Grossmann, M. Holschneider, R. Kronland-Martinet, J. Morlet, Detection of abrupt changes in sound signals with the help of wavelet transforms, in: Inverse Problems: An Interdisciplinary Study, Adv. Electr. Electr. Phys. (Supp. 19) (1987) 298–306.
[14] F.J. Herrmann, J.J. Staal, Waves in scaling media, the implication of non-differentiability, in: D.J. Feenstra (Ed.), 58th annual EAGE Conference, Amsterdam, 1996 (Abstract nr. C007).
[15] M. Holschneider, Wavelets: An Analysis Tool, Clarendon, Oxford, England, 1995, p. 423.
[16] E.R. Hughes, T.G. Leighton, G.W. Petley, P.R. White, Ultrasonic propagation in cancerous bone: a new stratified model, Ultrasound Med. Biol. 25 (1999) 811–821.
[17] G. Kaiser, Wavelet electrodynamics, Phys. Lett. A 168 (1992) 28–34.
[18] G. Kaiser, Wavelet electrodynamics: Atomic decomposition of electromagnetic waves, Appl. Comput. Harmon. Anal. 1 (1994) 246–260.
[19] G. Kaiser, Physical wavelets and radar: A variational approach to remote sensing, IEEE Antennas Propagation Mag. 38 (1996) 15–24.
[20] S. Mallat, W.L. Hwang, Singularity detection and processing with wavelets, IEEE Trans. Inf. Theory 38 (1992) 617–643.
[21] F. Moreau, D. Gibert, M. Holschneider, G. Saracco, Wavelet analysis of potential fields, Inverse Probl. 13 (1997) 165–178.
[22] Q.-Q. Ni, M. Iwamoto, Wavelet transform of acoustic emission signals in failure of model composites, Eng. Fracture Mech. 69 (2002) 717–728.
[23] M. Ohtsu, M. Shigeishi, Y. Sakata, Nondestructive evaluation of defects in concrete by quantitative acoustic emission and ultrasonics, Ultrasonics 36 (1998) 187–195.
[24] G. Saracco, Propagation of transient waves through a stratified fluid medium: Wavelet analysis of a nonasymptotic decomposition of the propagator. Part 1. Spherical waves through a two-layered system, J. Acoust. Soc. Am. 95 (1994) 1191–1205.
[25] K. Wapenaar, Amplitude variation with angle behavior of self-similar interface, Geophysics 64 (1999) 1928–1938.
[26] K. Wapenaar, Seismic reflection and transmission coefficients of a self-similar interface, Geophys. J. Int. 35 (1998) 585–594.
[27] R.S. Wu, X.L. Dong, J.H. Gao, Application of acoustic wavelet transform to seismic data processing, in: Society of Exploration Geophysicists, SEG 68th Annual Meeting, Expanded Abstracts, 1998, pp. 1987–1990.